Proceedings of the ASME 2016 International Design Engineering Technical Conferences and Computers and Information in Engineering Conference
IDETC/CIE 2016
August 21-24, 2016, Charlotte, North Carolina

DETC2016-59523

DESIGN AND PROTOTYPE OF A TUNABLE STIFFNESS ARM FOR SAFE HUMAN-ROBOT INTERACTION

Yu She
Department of Mechanical and Aerospace Engineering
The Ohio State University
USA, Columbus, Ohio 43210
ASME Student Member
Email: she.22@osu.edu

Hai-Jun Su *
Department of Mechanical and Aerospace Engineering
The Ohio State University
USA, Columbus, Ohio 43210
ASME Member, Associate Professor
Email: su.298@osu.edu

Cheng Lai
Department of Mechanical Engineering
Taiyuan University of Technology
Shanxi, Taiyuan, 030024, P.R. China
UG visiting scholar
Email:ChengLai15@gmail.com

Deshan Meng
Department of Mechanical and Automation
Shenzhen Graduate School, Harbin Institute of Technology
Guangdong, Shenzhen 518055, P.R. China,
Graduate visiting scholar
Email:dsmeng@hit.edu.cn

ABSTRACT

In this paper, we present a tunable stiffness robot link for safe human-robot interaction. Stiffness of a manipulator determines the injury levels of a human from an impact between robots and operators, given a specific impact velocity. Compliance of a robot manipulator includes joint compliance and link compliance. Variable stiffness design from the viewpoint of actuators have been widely studied, while adjustable stiffness robotic link in the application of human robot interaction is rare in literatures. This paper details the design of a tunable stiffness robotic manipulator via four bar linkages which are actuated by servo motors. A 3D model of the morphing beam is constructed, and a robot which is made up of 3 morphing arms is designed. Prototypes using 3D printer are fabricated. Numerous tests have been done, and the results show that the stiffness is able to change 3.6 times given a morphing angle of $\pi/4$. *Given an impact velocity of 2.2 m/s, the impact tests show that the acceleration has a 19.4% decrease comparing the curved beam and straight beam, and the head injury criteria (HIC) significantly decreases from 210.3* $m^{5/2}s^{-4}$ *to 150.3* $m^{5/2}s^{-4}$*, which is much safer to the operators. This paper explores the research of tunable stiffness on robotic links in the application of human robot interaction, expanding the research arena with regarding to human safe robot design.*

1 Introduction

Co-robots [1] have already been used in various environments: exoskeletons as human power amplifiers [2], haptic devices in virtual reality environments [3], rehabilitation [4, 5], and so on. With regard to manufacturing applications, co-robots have been developed as assistive devices in automotive industries [6]. Since humans and robots have complementary strengths, co-

*Address all correspondence to this author.

Copyright © 2016 by ASME

robots are particularly needed in accomplishing diff cult low-volume assembly tasks [7] in which human-robot collaboration is required. However, before co-robots can be pervasively used to work side-by-side with human workers, the issue of safety [8] must be addressed.

To evaluate the injury severity of the impact, several safety criteria, such as Head Injury Criterion (HIC), Gadd Severity Index (GSI), the Thoracic Trauma Index (TTI), the 3 m criterion, and the Viscous Injury Response (VC), from automotive and sports industries [9, 10] have been developed. A safety standard ISO10218 [11] states that one of the following requirement should be satisf ed for human robot interaction: the TCP (tool center point)/f ange velocity $\leq$ 0.25m/s, or dynamic power $\leq$ 80W, or static force $\leq$ 150N. The implementation of these standards is at the expenses of reduced performance and productivity.

Intuitively, a robot with a light weight and a low stiffness is relatively safe. Currently, a majority of work focuses on introducing compliance to the mechanical design. (1) Wrap robot arms with soft materials [12] to absorb impact energy. However, it has been estimated that a PUMA robot requires a compliant cover more than f ve inches in order to keep a tolerable HIC index of 100 at a velocity of 1m/s [13]. This solution is too bulky, hence resulting in a signif cantly reduced performance. (2) Employ compliant or soft materials for structural design [14, 15]. These designs have a low stiffness hence dramatically reduce effective inertia force. Compliant and passive (under-actuated) joints are commonly used in this approach. However, the biggest challenge of this approach is the severely reduced performance, e.g. poor positioning accuracy. (3) Novel actuator design [16]. Design of novel actuators for co-robot focuses on reducing inertia force of moving parts by using cable drives or pneumatic actuators [17]. However, these solutions suffer from low bandwidth, hence are limited to low performance tasks.

To gain high performance, a common solution is to use a variable stiffness actuator (VSA) which has a high stiffness in low speed and a low stiffness in high speed. For instance, COMAN (Compliant humanoid) [18] incorporates joints with variable stiffness that are actuated by passive compliance actuators based on the series elastic actuation principle. Zinn et al. [13] designed a distributed macro-mini actuation (DM2) which employs a pair of two actuators for the shoulder and elbow points, generating low and high frequency torque components respectively. Unfortunately, this solution adds extra complexity and costs. More importantly, the results of the impact test between a DLR-Lightweight Robot III (LWRIII) and a HIII Dummy shows that introducing compliance at joints does not affect the head impact considering the link inertia $\geq$ the one of the LWRIII [19].

Apart from design compliance on the actuator, researches introduce compliance in the link as well. Lpez-Martnez et al. [20] designed a f exible linkage for robot safe operation. The link remains a rigid part given the joint torque less than a threshold, but splits in two parts if the condition is not satisf ed. This approach ensures intrinsically safe operation for the co-robots. Park et al. [21] conduct similar work by designing a safe link mechanism. She et al. [22] proposed an inherently safe robotic arm by designing various stiffness distribution along the manipulator. However, all of these f exible link designs are passive and their stiffness are not controllable. Tunable stiffness beams have been proposed and used in a variety of applications such as legged robot [23],invasive surgery [24], f apping-wing robot [25]. But no applications on safe robot are found to the best understanding of the authors. Furthermore, there is lack of evaluations of injury regarding to the impact between a f exible link and an operator. She et al. [26] presents the injury calculation of a f exible link, but it has a constant stiffness along the beam.

In this paper, we propose a novel f exible robotic arm with turnable stiffness for safe robot interaction with humans. The stiffness of the robotic arm can be controlled high if the f ange velocity is low, from which the position accuracy and force control are not affected by the compliance. On the other hand, the stiffness can be turned low if the tip velocity is high and the safety concerns come to attention. The turnable stiffness is realized by the morphing shape of the beam, which is actuated by servo motors via four bar linkages. Numerous impact tests have been done to evaluate the injury level of the impact.

We begin this paper with an introduction of problem statement in Section 2. Design of the morphing arm is presented in Section 3. In Section 4, the detail design of the actuation mechanism of the morphing arm is given. Numerous experiment results are presented in Section 5. Finally, discussion and future work are presented in Section 6.

2 Problem statement

Unlike conventional industrial robots which are kept completely separated from humans to ensure safety, co-robots are designed to physically interact with humans in a shared workspace. As shown in Fig.1, conventional industrial robotic manipulators are designed to have a high stiffness due to the requirement for high performance, e.g. positioning accuracy and speed, in manufacturing automation. The safety concern is often addressed by control through sensing or caging. To ensure safety, performance must be sacrif ced signif cantly, e.g. reducing speed. On the other hand, soft robots made of soft materials and actuators have a high safety level. However, they do not offer the high performance required in many manufacturing tasks. Recently several human-safe co-robots have already emerged on the market. These co-robots rely on sensors to detect collision and then attempt to address this challenge by trading off the performance for safety. However, their performance or productivity is still far from meeting most manufacturing tasks in industry because of a signif cantly reduced performance. Therefore, a novel, high eff cient, and inherently safe robot (fast and safe robot) might be needed to develop.

Copyright © 2016 by ASME

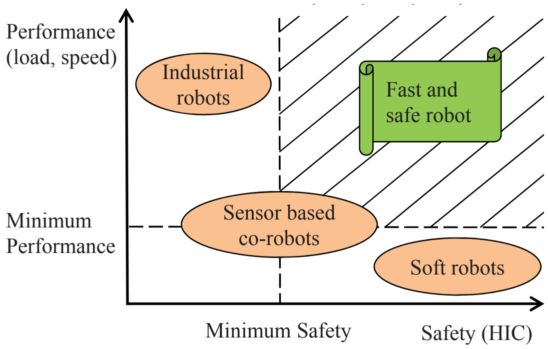

Figure 1 : Rough classif cation of robots considering safety and performance.

Considering a typical rest-to-rest task of an industrial robot, the motion might be divided into “start phase”, “intermediate phase”, and “end phase” as shown $v(t)$ in Fig.2. At the start phase, the robot starts to rotate with a speed of 0, and the speed gradually increases until it arrives at its maximum operation speed. Then it keeps its maximum operation speed during the intermediate phase. When it comes to the end phase, the robot’s speed is slowed down and the manipulator stops at the destination. The robot has a low speed at the start phase due to the inertia of the manipulator. High speed in the intermediate phase is desired to maximize the eff ciency. The robot has a low speed at the end phase since position or force control is usually desired at the destination.

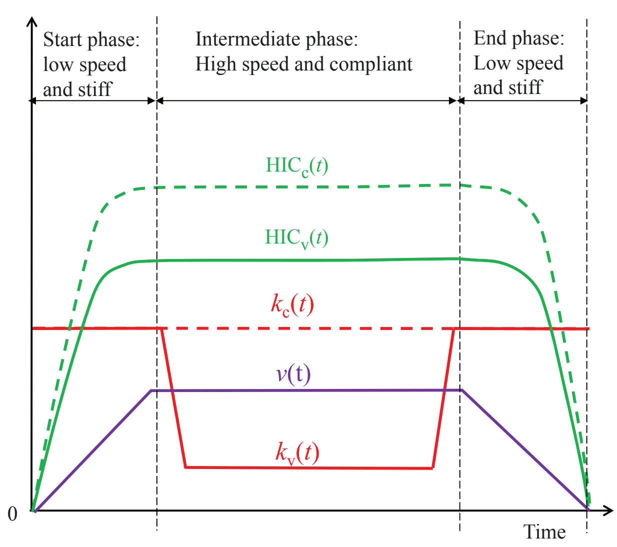

Figure 2 : Safety affected by tunable stiffness given a rest-to-rest task.

Intuitively, given a constant stiffness as $k_c(t)$ in Fig.2, a high speed of the manipulator might cause a heavily potential injury for humans, while a low speed maybe relatively safe. To hold eff ciency (high speed) and safety at the same time, one solution might reduce the stiffness of the beam. Therefore, part of the kinetic energy from the manipulator transfers to the strain energy in the arm, part of them transfers to dissipated energy, only the rest of them transfers to the kinetic energy to the operator which causes injury. One the other hand, high stiffness may be required at low speed considering the position accuracy and the force feedback control. Furthermore, the acceleration at the start and end phase might requires high stiffness of the robotic arm. Taken all of these into consideration, the desired stiffness of the robotic arm could be high-low-high as shown $k_v(t)$ in Fig.2.

To quantitatively measure injury severity, the head injury criterion (HIC) is used to evaluate the dynamic collision in this research. The HIC is def ned as [9]

$$\mathrm{HIC}(\Delta t_{max}) = \max_{\Delta t}\left\{\Delta t\left[\frac{1}{\Delta t}\int_{t_1}^{t_2}\hat{a}\,dt\right]^{2.5}\right\} \quad (1)$$
$$\text{subject to } \Delta t = t_2 - t_1 \leq \Delta t_{max}$$

where $\hat{a}(t)$ is the normalized acceleration of the operator’s head, i.e. $\hat{a} = a(t)/g$, $a(t)$ is the actual acceleration of the head, g is the gravitational constant, and (t_1, t_2) is the maximum impact interval. $\Delta t_{max} = 15$ ms and $\Delta t_{max} = 36$ ms are two widely used criterion and represented by HIC_{15} and HIC_{36}, respectively. Detailed discussion of HIC can refer [27], from which the limitations of the HIC to evaluate injury from robotic system are presented. Considering a mass-spring-mass impact system, Bicchi et al. [28] proposed an analytical expression of $\mathrm{HIC}_{36} = C_m k^{0.75} v^{2.5}$, where C_m is mass constant, k is the result stiffness, and v is the impact velocity. The HIC distribution with respect to $k_c(t)$ and $k_v(t)$ may be presented as $\mathrm{HIC}_c(t)$ and $\mathrm{HIC}_v(t)$, as shown in Fig.2 respectively. 10 times reduction of the stiffness could cause 5.6 times decreasing of the HIC value regarding to the mass-spring-mass system. Similar effect might apply to the a dynamic impact system comprised with a f exible arm-spring-mass. Therefore, the goal of this research is to design a tunable stiffness robotic arm to modulate the HIC to accommodate to different velocities, hence f nally to ensure the intrinsically safe operation for the manipulator.

3 Design of the morphing arm

A schematic diagram as shown in Fig.3 presents the working principle of the proposed robotic arm. The robotic arm comprised with two f exible arms (arm and forearm) each of which is made of two parallel compliant beams. These beams are morphed to a curved shape (stiff) by a servo motor at the start position v(0) = 0 for maximum acceleration. Then they are gradually restored to the f at shape (compliant) to ensure safety when the speed reaches the maximum v_{max}. At last, they are morphed back

Copyright © 2016 by ASME

to the curved shape for maximum deceleration till they reach the end position at $v(T) = 0$.

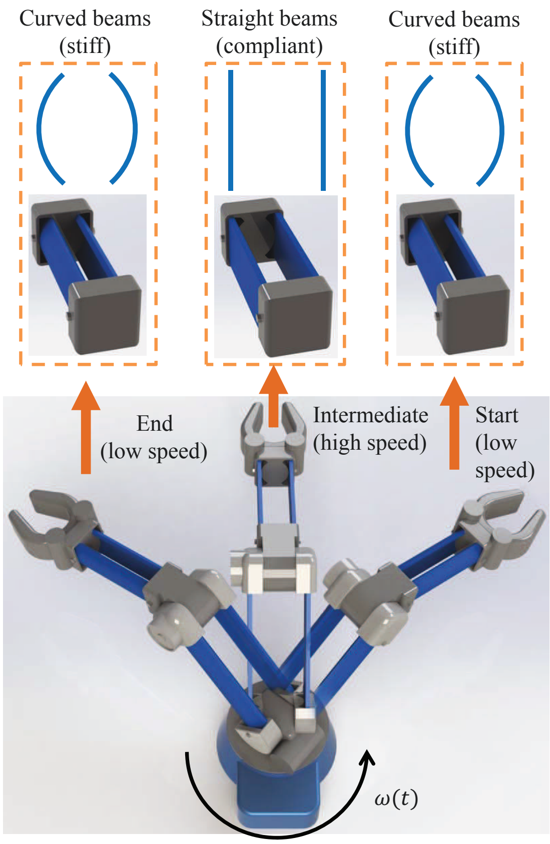

Figure 3 : A schematic diagram of the proposed morphing arm.

The actual design is shown in Fig.4. The manipulator is comprised with three flexible arms and three joints. The three robotic arms are forearm, arm, and trunk, while the three joints are at elbow, shoulder, and waist. The three links have the same compliant structure and provide compliance in 3 dimensions in space. The three joints offer the same function as the ones of the PUMA 560, i.e, any positions in its workspace can be reached via rotating the three joints. A counterbalance is mounted on the arm to balance the robotic arm.

The three compliant links have the same structure, and the detailed components of a flexible arm is as shown at the top of Fig.4. Two flexible beams are place on both sides of the arm and sit in the houses at both ends. The flexible beam with a crank-coupler mechanism form a four bar linkage, which is driven by a servo motor. The servo motor is mounted on the houses. At both ends of the flexible robotic arm, the house, the four bar linkage, and the servo motor are assembled in the same way. The compliant beams are designed with ribs to reduce the power of

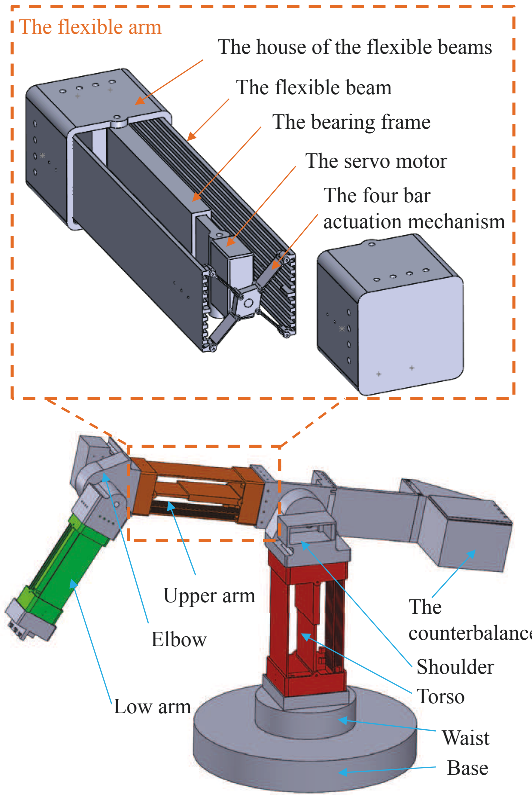

Figure 4 : The design of the proposed morphing manipulator.

morphing while to hold the lateral stiffness to some degree. A bearing frame is designed to connect the two houses between the compliant beams to support load in the vertical direction. It is a slide mechanism with two pivot joints mounted on both sides of the houses. Therefore, there is only one degree of freedom of the bearing frame, and the overall lateral stiffness of the flexible arm is not affected by the bearing frame.

The flexible arm is designed to have compliance in one direction (horizontal in this case) while rigid in the other direction (vertical in this case). The compliance can be achieved via morphing the shape of the flexible beam, in order to reduce the impact force on the operator. On the other hand, the rigidity can be obtained from the bearing frame whose stiffness does not change in vertical direction even though sliding in the bearing frame occurs during the morphing process, in order to support end load of the robot.

The flexible arm is actually a parallel guided beam as shown in Fig.5 (a), which can be regarded as a fixed-guided pseudo-rigid-body (PRB) model as shown in Fig.5 (b). The stiffness of each torsion spring of the fixed guided PRB model can be calculated by $K_{fg} = 2\gamma K_{\theta} E I_{fg}/L$, where γ is the characteristic radius factor, K_{θ} is stiffness coefficient, E, I_{fg}, and L are the young modulus, moment of inertia, and length of the flexible

Copyright © 2016 by ASME

arm, respectively.

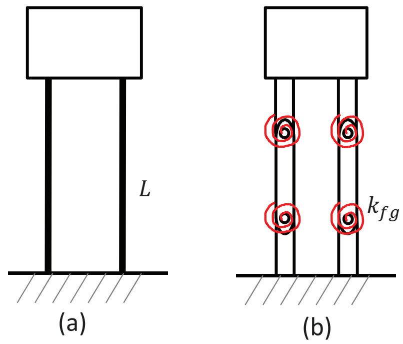

Figure 5 : (a) The parallel guided f exible beam, (b) The f xed-guided PRB model of the f exible robotic link.

4 Design of the actuation mechanism

The two morphing beams are actuated by eight pairs of four bar linkages, with fours pairs on each side. Fig.6 shows the two typical positions of the actuation mechanism. The beam is f at and compliant in Fig.6 (a), and is curved and stiff in Fig.6 (b). The f exible beam is f xed at the middle of its bottom face. Both sides of its tip are pinned to rigid links, and the links are pinned on a disk. The disk can be driven by the servo motor. The f exible beam deforms as a cantilever beam given actuation from the disk.

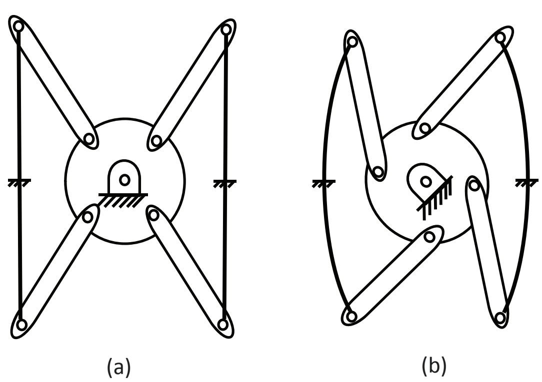

Figure 6 : (a) The actuation mechanism at the f at beam shape, (b) The actuation mechanism at the curved beam shape.

A single four bar mechanism designed in this research is shown in Fig.7 (a). The f exible cantilever beam can be approximated by a PRB model, and the approximated four bar linkage is shown in Fig.7 (b). Assuming the height of the f exible beam is l, the inertia of moment of the cantilever beam is I_c, the characteristic radius of the PRB model is $r_4 = \gamma l$, and the stiffness of the cantilever beam is calculated as $K_c = \gamma K_\theta E I_c / l$. Therefore, the compliant actuation mechanism can be transferred to a traditional rigid four bar linkage, and kinematics of the four bar linkage can be used to optimize the length of each link.

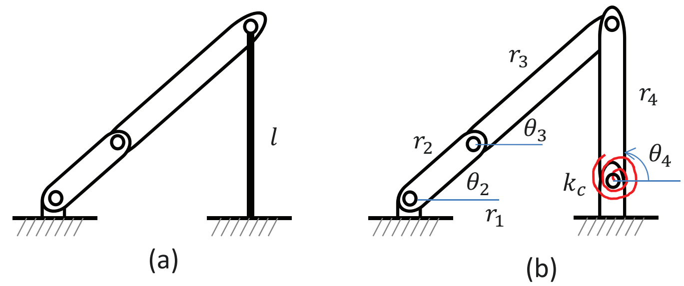

Figure 7 : (a) The four bar actuation mechanism, (b) The PRB model of the four bar linkage.

Given a specif c rotation direction of the disk (eg. CCW), it is observed that there are two branches of the four bar linkages, based on the Fig.6 (b). The diagonal four bar linkages could have the same dimensions since they are in the branch, while the adjacent four bar linkages could have different dimensions since they are under different branches. In this research, the dimensions of the two different branches of the four bar linkage are designed to achieve a symmetric shape of the f exible beam at a specif ed shape. In other words, given the same crank angle of θ_2, it is desired to obtain the same rocker angel of θ_4, for different branches of the four bar linkage. Some dimensions or constrains are given as follows: $r_1 = 25$ mm, $l = 25$ mm, $r_2 + r_3 = 35$ mm, $\theta_{20} = \theta_{30} = \pi/4$, $\theta_{40} = \pi/2$. The problem statement is as follows: given an absolute rotation angle of $\theta_2^1 = \alpha$ for branch 1 and $\theta_2^2 = -\alpha$ for branch 2, it is desired to have the same rocker angle of branch 1 and 2, i.e. $\theta_4^1 = \theta_4^2$. To explore the appropriate dimensions of the links, considering $\alpha = \pi/4$ and $r_2 = 10$ mm for branch 1, the kinematics analysis for a certain length of r_2^1 and a variety of r_2^2 is presented as shown in Fig.8. It is observed that $r_2^2 = 8$ mm could satisfy the requirement. After quantifying the dimensions of the four bar linkage, a prototype of the f exible robotic manipulator was fabricated and numerous tests have been conducted to explore its performance.

5 Experiment

A 3 armed robotic manipulator is fabricated, and all parts are fabricated by a 3D printer with ABS plastic material. A single f exible robotic arm is shown in Fig. 9 (a), and the three armed robotic manipulator is shown in Fig.9 (b). In Fig.9 (a), the f exible arm is mounted on a f ange which can be f xed to the axis of a

Copyright © 2016 by ASME

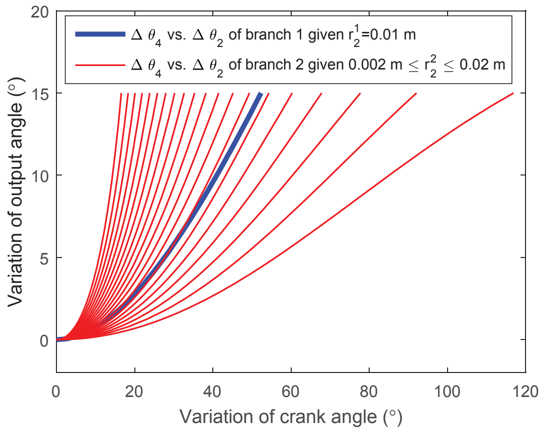

Figure 8 : Exploration of the kinematics of the two branches of the four bar linkage.

servo motor, and most of the impact tests are based on the single f exible robot link. In Fig.9 (b), three f exible arms are assembled together to provide compliance in three dimensions. The rotation from the waist, shoulder and wrist enable the end of the forearm reach to any position in its workspace. A DC motor (2.5” CIM Motor) is placed at the waist, and two ultra high torque servo motor (HD-1235MG) are placed at the shoulder and wrist, respectively. In addition, two servo motors (HS-81) are placed on both side of each link to morph the f exible beam.

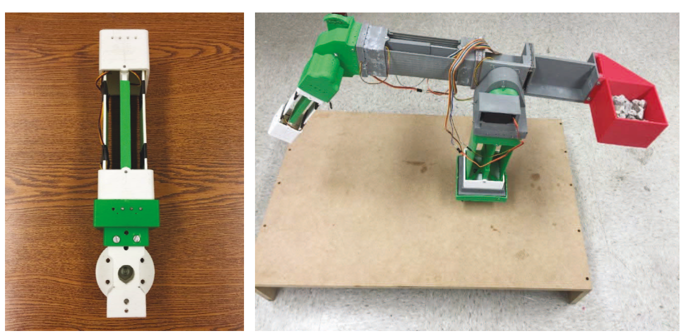

(a) (b)

Figure 9 : (a) A 3D printed f exible arm, (b) The 3D printed robotic manipulator

The stiffness test has been conducted after the robotic link has been fabricated and assembled. The experiment setup of the stiffness test is as shown in Fig.10. The morphing arm is clamped to a f xture on one end. A high resolution force sensor (PASCOs PS-2189) is f xed on the platform of a CNC mill, and the sensor contacts the other end of the f exible arm. Therefore, given displacement command from the CNC mill, its platform pulls the other end of the f exible arm and deforms the arm. Therefore, the displacement of the link can be represented by that of the platform of the CNC mill, which is monitored by a displacement sensor (PASCOs PS-2204). A data collection and analysis device (PASCOs PS-2008A) is used to access data from the sensors. The motion of the platform of the CNC mill is controlled by a computer (not shown). A laptop is used to update the program of the micro-controller. A morphing angle (β) is def ned as the entire deformation angle of the f exible beam. The morphing angle is driven by two servo motors, which are controlled by a micro-controller.

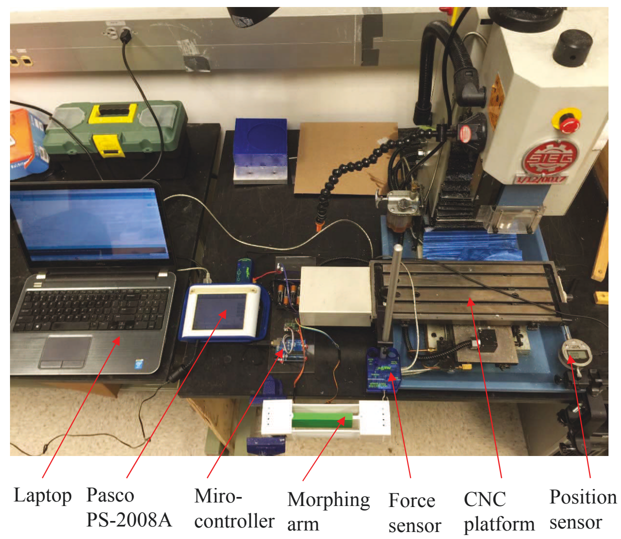

Figure 10 : The experiment setup of the stiffness test.

The stiffness testing results are shown in Fig.11. After the applied force (F) and corresponding displacement (δ) are read from the sensors, one might calculate the lateral stiffness using $k_l = F/\delta$. In this test, different morphing angles are tested and controlled by the servo motors, and the slopes represent the stiffness of the f exible arm at a specif c morphing angle. The morphing angle are increased from 0 to $\pi/4$ degree, and the stiffness increases from 0.54 N/mm to 1.936 N/mm. The maximum stiffness ($\beta = \pi/4$) is 3.6 times of the smallest stiffness ($\beta = 0$).

Followed by the stiffness tests, numerous impact tests are conducted to show the effect of the link compliance on the impact. The impact experiment setup is shown in Fig.12. The DC motor is mounted on the platform, and it is controlled by a micro-controller via a separate speed controller. An encoder is mounted on the output axis of the motor to monitor the position of the motor (hence the angular velocity), and the data are collected and stored to the micro-controller. The morphing arm is mounted on and driven by the DC motor. An end effector is clamped at the end of the morphing arm to lengthen the arm in order to hit a

Copyright © 2016 by ASME

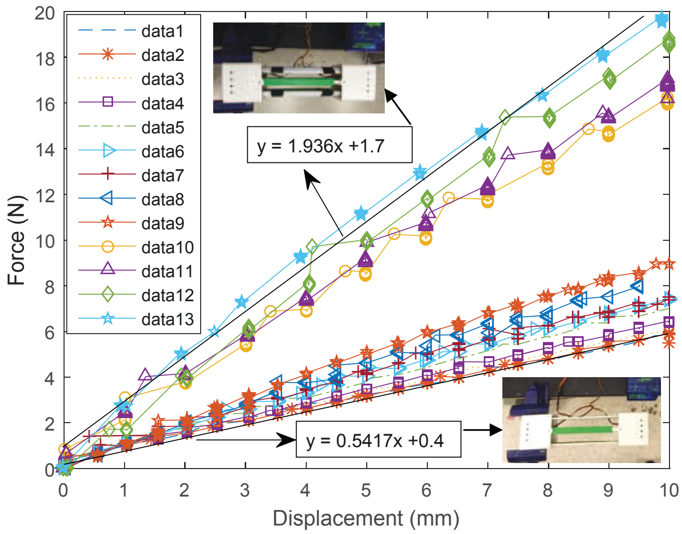

Figure 11 : The stiffness testing results

cargo, which is placed on a frictionless slide trail (PAStrack Dynamics System ME-6962). An 3-axis acceleration sensor (PASCOs PS-2136A) is f xed on the cargo to monitor the acceleration. The acceleration data is stored by the data collection and analysis device. A force sensor is placed in the front of the cargo to detect the impact, and the force information is monitored and stored by the micro-controller. A Stanley level is used to make sure the slide trail is horizontal.

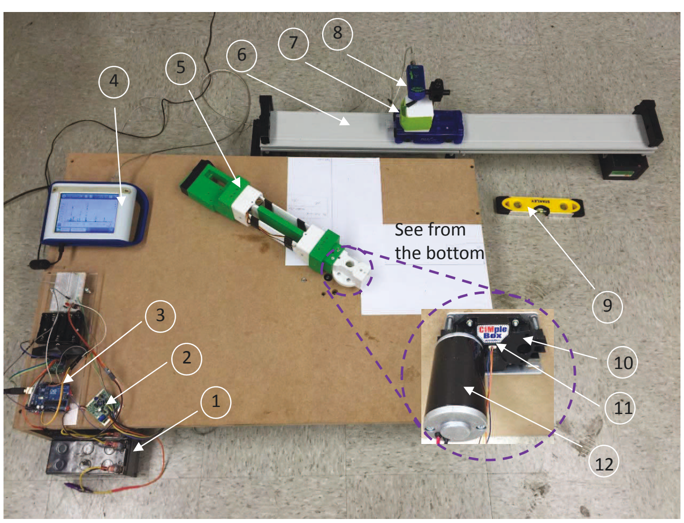

1. Power supply, 2. Speed controller, 3. Micro-controller, 4. PASCO PS-2008A, 5. Morphing arm, 6. PAStrack Dynamics System ME-6962, 7. Force sensor, 8. Acceleration sensor, 9. Stanley Level, 10. Gear box, 11. Encoder, 12. DC motor

Figure 12 : The impact experiment setup.

The impact test with different impact velocities is shown in Fig.13. The sampling frequency of the sensors is set to be 500 Hz. In this test, repetitive tests are conducted for each certain given speed, and the results show that the test may be basically trusted. The impact velocities in this f gure are set to be $v_1 = 1.8$ m/s, $v_2 = 1.93$ m/s, and $v_3 = 2.2$ m/s respectively, and the peaks of the corresponding accelerations are 11.41 m/s^2, 36.97 m/s^2, and 56.7 m/s^2, as shown in Fig.13. It is observed that the impact period is very short and the impact interval is usually less than 30 ms. The impact acceleration is signif cantly affected by the impact velocity, while the impact cycle is slightly affected. The higher the velocity, the higher the impact acceleration and the shorter the impact interval.

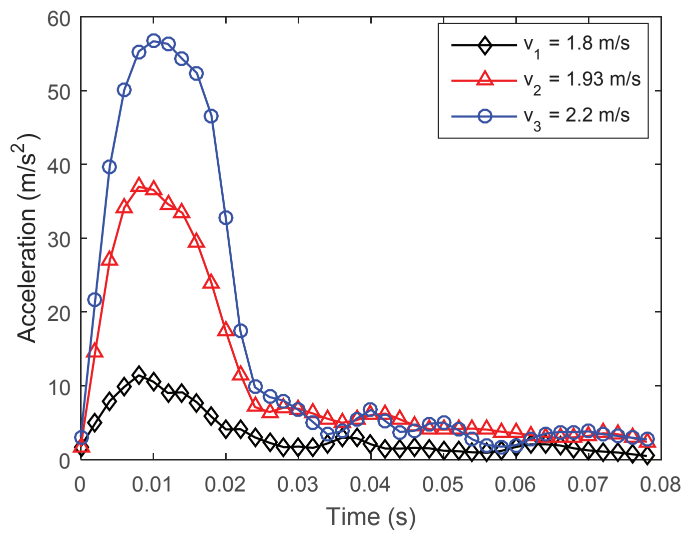

Figure 13 : Impact tests with different impact velocities.

The impact test with different stiffness tests is shown in Fig.14. In this test, the impact speed is f xed as 2.2 m/s, but the stiffness of the compliant robotic arm is controlled with the minimum and the maximum value. It is observed that 19.4 % decrease of the impact acceleration is obtained. The peaks of the corresponding accelerations are 45.71 m/s^2 and 56.7 m/s^2, respectively. The HIC values are calculated of 150.3 m$^{5/2}$s^{-4} and 210.3 m$^{5/2}$s^{-4} according to Eq. (1). The HIC value of the soft impact is 71% that of the hard impact, considering the minimum stiffness and the maximum stiffness, respectively. It is observed that the impact interval of the soft impact is slight larger than that of the hard impact.

6 Discussion and future work

The contribution of this work is to introduce the compliance to the robotic arm for the application of human robot interaction.

Copyright © 2016 by ASME

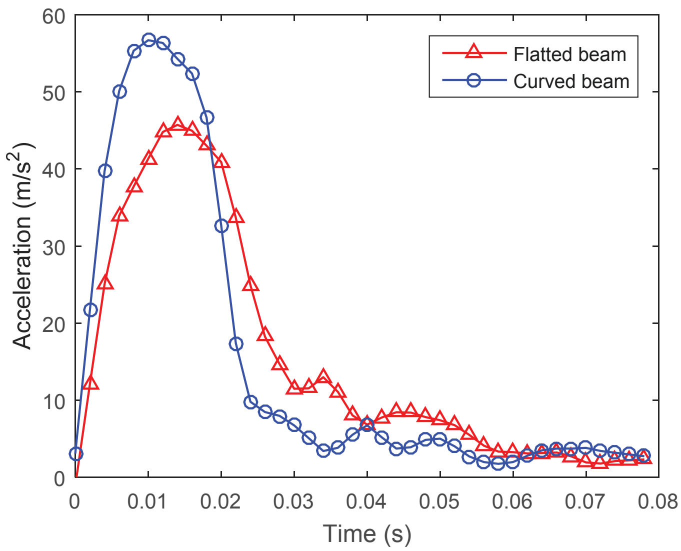

Figure 14 : Impact tests with different arm stiffness.

This paper details the design of a compliant robotic manipulator. The principle of the stiffness variation is to control the moment of inertia of the cross area of the robotic arm. This is realized by morphing the shape of the f exible robotic beam. A 3D printed f exible robotic manipulator is fabricated. Extensive tests regarding to the variation of stiffness and impact performance are conducted on a single f exible robotic arm.

The preliminary tests show that the possibility to reduce impact injury by introducing compliance into the robotic link. To make a solid conclusion, a few improvements of the impact tests could be addressed in the future. First, the sampling frequency of the sensors in this test is not high enough to precisely evaluate the impact result. The HIC value might be signif cantly affected by the sampling frequency since it is calculated the integral of the acceleration with time. A new data acquisition system with much higher sampling frequency is going to be used to resolve this problem. Second, the motor controller of the DC motor do not guarantee the precise velocity control. A slightly different velocity might have a large effect on the impact result according to the expression of HIC presented in section 2. An alternative method with accurate velocity control will be studied in the future research. Third, the anisotropy of the ABS material might be another factor to introduce error to the result. A metal compliant robotic arm might be better to get rid off this issue. Finally, the impact tests with three armed robotic manipulator should be conduct to explore the three dimensional compliance in space.

REFERENCES

[1] Colgate, J. E., Edward, J., Peshkin, M. A., and Wannasuphoprasit, W., 1996. "Cobots: Robots for collaboration with human operators".

[2] Chu, A., Kazerooni, H., and Zoss, A., 2005. "On the biomimetic design of the berkeley lower extremity exoskeleton (bleex)". In Robotics and Automation, 2005. ICRA 2005. Proceedings of the 2005 IEEE International Conference on, IEEE, pp. 4345–4352.

[3] Frisoli, A., Rocchi, F., Marcheschi, S., Dettori, A., Salsedo, F., and Bergamasco, M., 2005. "A new force-feedback arm exoskeleton for haptic interaction in virtual environments". In Eurohaptics Conference, 2005 and Symposium on Haptic Interfaces for Virtual Environment and Teleoperator Systems, 2005. World Haptics 2005. First Joint, IEEE, pp. 195–201.

[4] Roderick, S., and Carignan, C., 2007. *Designing safety-critical rehabilitation robots*. Citeseer.

[5] Wolbrecht, E. T., Chan, V., Reinkensmeyer, D. J., and Bobrow, J. E., 2008. "Optimizing compliant, model-based robotic assistance to promote neurorehabilitation". *Neural Systems and Rehabilitation Engineering, IEEE Transactions on,* **16**(3), pp. 286–297.

[6] Yamada, Y., Konosu, H., Morizono, T., and Umetani, Y., 1999. "Proposal of skill-assist: a system of assisting human workers by ref ecting their skills in positioning tasks". In Systems, Man, and Cybernetics, 1999. IEEE SMC'99 Conference Proceedings. 1999 IEEE International Conference on, Vol. 4, IEEE, pp. 11–16.

[7] Kaipa, K. N., Morato, C., Liu, J., and Gupta, S. K., 2014. "Human-robot collaboration for bin-picking tasks to support low-volume assemblies". In Human-Robot Collaboration for Industrial Manufacturing Workshop, held at Robotics: Science and Systems Conference (RSS 2014).

[8] Bicchi, A., Peshkin, M. A., and Colgate, J. E., 2008. "Safety for physical human–robot interaction". In *Springer handbook of robotics*. Springer, pp. 1335–1348.

[9] Versace, J., 1971. A review of the severity index. Tech. rep., SAE Technical Paper.

[10] Newman, J. A., Shewchenko, N., and Welbourne, E., 2000. "A proposed new biomechanical head injury assessment function-the maximum power index.". *Stapp car crash journal,* **44**, pp. 215–247.

[11] ISO10218-1:2006, 2006. *Robots for Industrial Environments - Safety Requirements. Part I: Robot*. International Organization for Standarization.

[12] Iwata, H., Hoshino, H., Morita, T., and Sugano, S., 2001. "Force detectable surface covers for humanoid robots". In Advanced Intelligent Mechatronics, 2001. Proceedings. 2001 IEEE/ASME International Conference on, Vol. 2, IEEE, pp. 1205–1210.

[13] Zinn, M., Roth, B., Khatib, O., and Salisbury, J. K., 2004. "A new actuation approach for human friendly robot design". *The international journal of robotics research,* **23**(4-5), pp. 379–398.

Copyright © 2016 by ASME

[14] Shepherd, R. F., Ilievski, F., Choi, W., Morin, S. A., Stokes, A. A., Mazzeo, A. D., Chen, X., Wang, M., and Whitesides, G. M., 2011. "Multigait soft robot". *Proceedings of the National Academy of Sciences,* **108**(51), pp. 20400–20403.
[15] Tolley, M. T., Shepherd, R. F., Mosadegh, B., Galloway, K. C., Wehner, M., Karpelson, M., Wood, R. J., and Whitesides, G. M., 2014. "A resilient, untethered soft robot". *Soft Robotics,* **1**(3), pp. 213–223.
[16] Filippini, R., Sen, S., and Bicchi, A., 2008. "Toward soft robots you can depend on". *Robotics & Automation Magazine, IEEE,* **15**(3), pp. 31–41.
[17] Ham, R. v., Sugar, T. G., Vanderborght, B., Hollander, K. W., and Lefeber, D., 2009. "Compliant actuator designs". *Robotics & Automation Magazine, IEEE,* **16**(3), pp. 81–94.
[18] Tsagarakis, N. G., Morfey, S., Cerda, G. M., Zhibin, L., and Caldwell, D. G., 2013. "Compliant humanoid coman: Optimal joint stiffness tuning for modal frequency control". In Robotics and Automation (ICRA), 2013 IEEE International Conference on, IEEE, pp. 673–678.
[19] Haddadin, S., Albu-Schäffer, A., and Hirzinger, G., 2009. "Requirements for safe robots: Measurements, analysis and new insights". *The International Journal of Robotics Research,* **28**(11-12), pp. 1507–1527.
[20] López-Martínez, J., Blanco-Claraco, J. L., García-Vallejo, D., and Giménez-Fernández, A., 2015. "Design and analysis of a f exible linkage for robot safe operation in collaborative scenarios". *Mechanism and Machine Theory,* **92**, pp. 1–16.
[21] Park, J.-J., Kim, B.-S., Song, J.-B., and Kim, H.-S., 2008. "Safe link mechanism based on nonlinear stiffness for collision safety". *Mechanism and Machine Theory,* **43**(10), pp. 1332–1348.
[22] She, Y., Su, H.-J., and Hurd, C. J., 2015. "Shape optimization of 2d compliant links for design of inherently safe robots". In ASME 2015 International Design Engineering Technical Conferences and Computers and Information in Engineering Conference, American Society of Mechanical Engineers, pp. V05BT08A004–V05BT08A004.
[23] Galloway, K. C., Clark, J. E., and Koditschek, D. E., 2013. "Variable stiffness legs for robust, eff cient, and stable dynamic running". *Journal of Mechanisms and Robotics,* **5**(1), p. 011009.
[24] Kim, Y.-J., Cheng, S., Kim, S., and Iagnemma, K., 2013. "A novel layer jamming mechanism with tunable stiffness capability for minimally invasive surgery". *Robotics, IEEE Transactions on,* **29**(4), pp. 1031–1042.
[25] Hines, L., Arabagi, V., and Sitti, M., 2012. "Shape memory polymer-based f exure stiffness control in a miniature f apping-wing robot". *Robotics, IEEE Transactions on,* **28**(4), pp. 987–990.
[26] She, Y., Meng, D., Shi, H., and Su, H.-J., 2015. "Dynamic modeling of a 2d compliant link for safety evaluation in human-robot interactions". In Intelligent Robots and Systems (IROS), 2015 IEEE/RSJ International Conference on, IEEE, pp. 3759–3764.
[27] Gao, D., and Wampler, C., 2009. "Head injury criterion". *IEEE Robotics Automation Magazine,* **16**(4), Dec., pp. 71–74.
[28] Bicchi, A., and Tonietti, G., 2004. "Fast and" soft-arm" tactics [robot arm design]". *Robotics & Automation Magazine, IEEE,* **11**(2), pp. 22–33.

Copyright © 2016 by ASME